JACS
JOURNAL OF THE AMERICAN CHEMICAL SOCIETY
pubs.acs.org/JACS
Article

Quantitative Localized Analysis Reveals Distinct Exosomal Protein-Specific Glycosignatures: Implications in Cancer Cell Subtyping, Exosome Biogenesis, and Function

Yuna Guo, Jing Tao, Yiran Li, Yimei Feng, Huangxian Ju, Zhongfu Wang, and Lin Ding*

Cite This: J. Am. Chem. Soc. 2020, 142, 7404–7412
Read Online

ABSTRACT: Protein-specific glycoform analysis is essential for the thorough understanding of cellular chemistry and signaling but presents a significant assay challenge for small-sized, free-floating exosomes, ubiquitous regulators of cellular physiological functions and mediators of intercellular communication. We report herein a quantitative localized analysis (QLA) method for the first-time achievement of a protein-specific glycosignature assay on these important extracellular vesicles. The integration of localized chemical remodeling and quantitative electrochemistry allows the proof-of-concept QLA examination of exosomal mucin 1 (MUC1)-specific terminal galactose/*N*-acetylgalactosamine (Gal/GalNAc). In combination with sialic acid (Sia) cleavage manipulation for the exposure of originally capped Gal/GalNAc, QLA has revealed distinct MUC1-specific sialylation capping ratios for MCF-7 and MDA-MB-231 exosomes, as well as when compared to parent cells. These findings suggest a useful noninvasive indicator for subtyping cancer cells and exosome secretion as a likely venue for the preservation of cellular compositional and functional integrity. The QLA method also permits dynamic monitoring of changes in the exosomal MUC1-specific sialylation capping ratio, enabling the distinction of biogenesis pathways of exosomes.

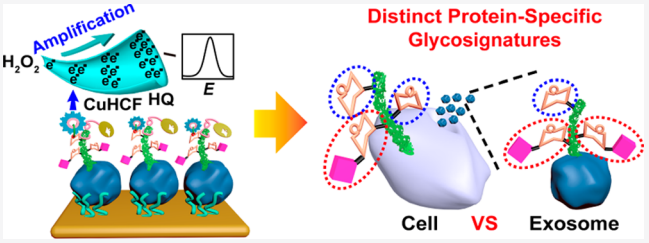

INTRODUCTION

Exosomes are extracellular vesicles secreted by cells, typically in the range of 40 to 150 nm,[1] through an intracellular endocytic trafficking pathway.[2] These membrane-bound structures, conserved across all kingdoms of life, have been increasingly recognized as ubiquitous regulators of cellular physiological functions (e.g., waste disposal)[3] and mediators for intercellular communication (e.g., immune signaling,[4] neurotransmission,[5] tumorigenesis[6]). Innovative diagnostic and therapeutic applications have emerged accompanying the discoveries.[7,8] To fully explore the biological implications and clinical utility of exosomes, a foundational prerequisite is the precise understanding of their compositional organization. In this regard, a focused set of lipids (e.g., cholesterol),[9] nucleic acids (e.g., mRNA, microRNA),[10] and proteins (e.g., HSP90)[11] have been identified, in certain cases, in an enriched form in exosomes as compared to parent cells. These covalently well-defined species provide a straightforward mechanistic basis for prescribing a suite of functional roles for exosomes.[12]

Glycosylation, featuring covalently complex linkages and proving versatile in regulating myriad physiological and disease processes at the cellular level,[13] can serve as a more flexible handle for leveraging the diversified potentials of exosomes.[14] The original speculation that the molecular composition on exosomes may represent that on resident cells is challenged by the finding that several glycoforms are enriched (high mannose, polylactosamine, *a*2,6-linked sialic acid (Sia), complex *N*-linked glycans (*N*-glycans), etc.) or depleted (terminal blood group A and B antigens, etc.) on the exosomal surface relative to the parent cells.[15] This somewhat surprising phenomenon has driven enormous interest into the study of exosomal glycosylation. However, thus far, only the ensemble state of glycosylation has been examined for exosomes on a global scale.[16−18] To elucidate the elaborate regulation mechanisms of glycosylation on the exosomal sorting and subsequent functions (interaction with and uptake by other cells) at the individual protein level, it is of vital importance to scrutinize the detailed exosomal glycosignatures in an *in situ* and protein-specific manner, but no investigative tool has been developed.

Indeed, several challenges are immediately apparent considering the small-sized, free-floating nature of exosomes. With respect to the confinement of analysis to a specific exosomal protein, one needs to respectively tag the protein and the glycans of interest; however, the existing cellular glycan labeling techniques, including metabolic glycan labeling[19] and localized chemical remodeling,[20] are problematic in the context

Received: November 11, 2019
Published: April 2, 2020

https://dx.doi.org/10.1021/jacs.9b12182
J. Am. Chem. Soc. 2020, 142, 7404−7412

Scheme 1. Schematic Illustration of Quantitative Localized Analysis (QLA) for the Assay of Protein-Specific Glycosignatures on Exosomes[a]

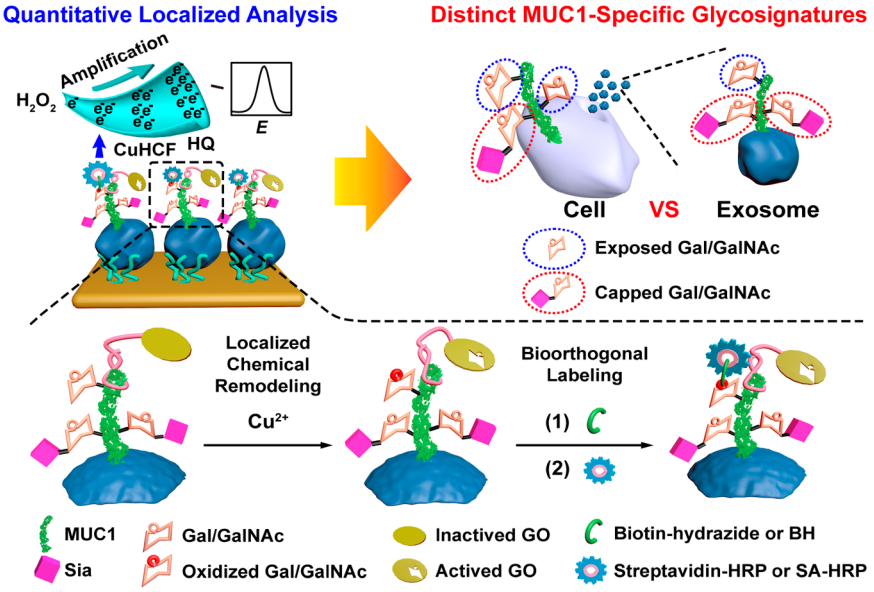

[a]Through glycan remodeling by target protein mucin 1 (MUC1)-confined galactose oxidase (GO), a redox-active horseradish peroxidase (HRP) is coupled to exosomal MUC1. By virtue of the electron shuttle property of copper hexacyanoferrate (CuHCF) and hydroquinone (HQ), *in situ* electrochemical examination of MUC1-specific galactose/*N*-acetylgalactosamine (Gal/GalNAc) is achieved, which reveals distinct glycosignatures between the exosomes and parent cells.

of the study of exosomes: (1) the ability and efficiency to sort proteins harboring metabolic glycan labels to small-sized exosomes have not been systematically confirmed, rendering the utility of a metabolic glycan labeling-based, trans-[21] or cis-membrane[22] protein-confined Förster resonance energy transfer method potentially infeasible; (2) the free-floating nature of exosomes makes direct application of protocols developed on adherent mammalian cells problematic; for example, the supposedly localized chemical remodeling[20] event can be unintendedly imposed on nonspecific targets due to the solution-phase collision of exosomes. From the perspective of *in situ* analysis, (1) the small-sized exosomes are beyond the diffraction limit of typical optical microscopy and cannot be approached by conventional fluorescence imaging;[23] also, fluorescence imaging can provide only qualitative or, at best, semiquantitative information,[24] (2) the small size of exosomes also implies a limited pool of each type of glycoproteins, and therefore, fluorescent intensity measurement (e.g., flow cytometry, or FCM) can require the concentration of an impractically high quantity of exosomes,[25] and (3) the surface confinement of exosomes needs to be coupled with an appropriate surface-confined readout format; in this regard, the buildup of a sufficient quantity of surface-confined fluorescent species can be a daunting task.

With these challenges in mind, herein we report an effective quantitative localized analysis (QLA) method for the first-time achievement of an *in situ* protein-specific glycosignature assay on exosomes (Scheme 1). In particular, quantitative electrochemistry has been exploited for interrogating the electrode interface-confined, protein-localized carbohydrate remodeling event to constitute a highly sensitive analytical platform involving a minimum quantity of exosomes. The development of such an enabling tool relies on a distinguished feature of electrochemistry over other assay formats, the requirement of a single surface-confined electroactive component, even at localized sites, for mediating the cascade electron transfer processes from solution-phase species to generate amplified signal (reflecting an exosomal remodeled carbohydrate site on the protein of interest), thus vastly simplifying the surface assay architecture. In brief, an electrode-confined, high-affinity aptamer is used to capture the exosomes of interest; localized chemical remodeling (i.e., guiding an inactivated glyco-editing enzyme to the target protein by a target-specific aptamer, followed by activation of the enzyme for proximity catalysis-enabled protein-specific glyco-remodeling) is performed on the target glycoprotein for coupling with a redox-active enzyme; the localized redox-active enzyme, along with other redox-active species in the solution phase (as well as on the surface), acts as an electron shuttle for QLA electrochemistry. Significantly, in combination with glycan chain cleavage manipulation, QLA of exosomes has revealed, for the first time, protein-specific glycosignatures distinct from those of parent cells (Scheme 1), which suggests a useful noninvasive indicator for subtyping cancer cells and exosome secretion as a likely venue for the preservation of cellular compositional and functional integrity. The QLA also permits dynamic monitoring of changes in the exosomal protein-specific glycosignatures upon glycan manipulation on parent cells, which provides direct evidence for the biogenesis pathway of exosomes.

RESULTS AND DISCUSSION

Characterization of Exosomes. We commenced our investigation on the feasibility of QLA by isolating exosomes from three breast cell lines: MCF-7 (tumorigenic human breast epithelial cells; the corresponding exosomes are abbreviated as MCF-7 exosomes hereafter), MDA-MB-231 (triple negative, tumorigenic human breast epithelial cells), and MCF-10A (nontumorigenic human breast epithelial cells).[26] The purification proceeds through an established differential centrifugation approach.[26] Transmission electron microscopy

https://dx.doi.org/10.1021/jacs.9b12182
J. Am. Chem. Soc. 2020, 142, 7404−7412

(TEM) shows a cup-shaped morphology and a size range of approximately 30 to 140 nm (Figure 1a–c), consistent with

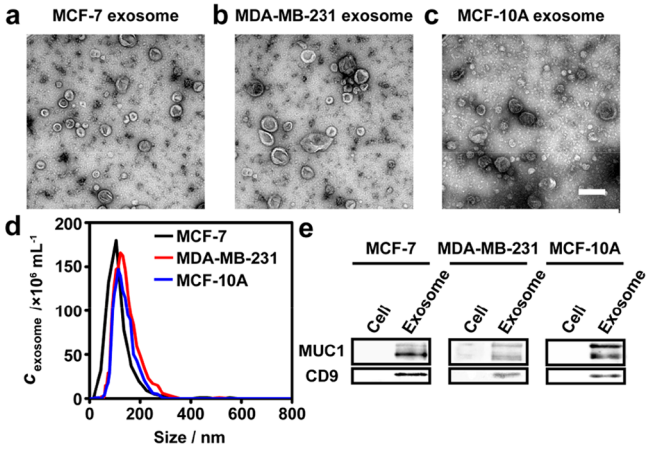

Figure 1. Characterization of exosomes. Imaging of exosomes by negative staining TEM: (a) MCF-7, (b) MDA-MB-231, (c) MCF-10A. Scale bar: 200 nm. (d) NTA for determination of exosome concentration ($c_{exosome}$) and size distribution. (e) Western blot analysis of MCF-7, MD-MBA-231, and MCF-10A cell and exosome lysates using anti-MUC1 and anti-CD9 antibodies.

literature-reported characteristics for exosomes.[1,27] Accordingly, nanoparticle tracking analysis (NTA) presents a narrow size distribution centered at 113.8, 132.5, and 126.5 nm, respectively, for MCF-7, MDA-MB-231, and MCF-10A exosomes (Figure 1d). The exosome identity is further validated by the Western blot observation of classical marker protein CD9 (Figure 1e).[26] In addition, an important, abundantly expressed transmembrane glycoprotein bearing a heavily *O*-glycosylated variable number tandem repeat (VNTR) domain, mucin 1 (MUC1),[28] has also been detected (Figure 1e) and selected as our QLA target because it is overexpressed in most epithelial cancers and is widely regarded as an oncogenic molecule.

Assembly and Investigation of QLA Surface Architecture. The layer-by-layer assembly of QLA surface architecture was then carried out on a Au electrode (AuE) using MCF-7 exosomes as the proof-of-concept system. Cyclic voltammetry (CV) (Figure 2a) and electrochemical impedance spectroscopy (EIS) (Figure 2b) are used for monitoring the assembly steps by virtue of the sensitive response of the electron transfer process to the composition change of the electrode surface. With $[Fe(CN)_6]^{3-}/[Fe(CN)_6]^{4-}$ as the redox probe pair, the bare AuE displays a pair of reversible electron transfer redox peaks (CV) and a diffusion-limited, linear Nyquist plot (EIS). The assembly of an aptamer (5′-modified with a thiol group for interacting with the Au surface, abbreviated as 5′-SH-apt1; all DNA sequences read from 5′ to 3′) targeting EpCAM (a transmembrane glycoprotein exclusively expressed in epithelial cells and a representative surface marker of exosomes)[29] on MCF-7 exosomes blocks the electron transfer process, as evidenced by reduced peak currents and increased separation of peak potentials (CV) as well as the appearance of a kinetics-characterizing, semicircular region (EIS). The electron transfer process becomes more sluggish with the passivation of the electrode surface by 6-mercapto-1-hexanol (MCH), the capturing of exosomes, and the blocking of nonspecific interactions by bovine serum

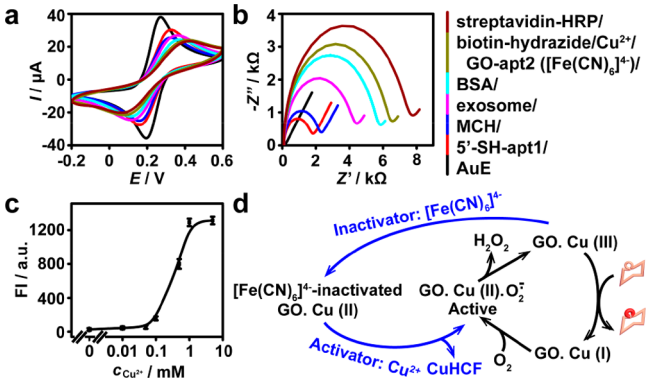

Figure 2. Monitoring of layer-by-layer assembly of QLA surface architecture on the AuE for MCF-7 exosomes: (a) CV, (b) EIS. (c) Cu^{2+} as an activator of $[Fe(CN)_6]^{4-}$-inactivated GO, as evaluated with the standard GO toolkit, showing Cu^{2+} concentration-dependent recovery of GO activity. (d) Schematic diagram for inhibition of GO activity by $[Fe(CN)_6]^{4-}$ and subsequent activation by Cu^{2+}.

albumin (BSA). Further localized chemical remodeling, executed by initial binding of GO-apt2 (a conjugate of galactose oxidase and MUC1-targeting aptamer,[30] with GO inactivated by $[Fe(CN)_6]^{4-}$) to MUC1 and subsequent MUC1-specific oxidation of terminal galactose/*N*-acetylgalactosamine (Gal/GalNAc) from the C6-hydroxy to the aldehyde group (GO activated by Cu^{2+}), enables bioorthogonal labeling of biotin-hydrazide and binding of streptavidin-HRP (horseradish peroxidase). These events can also be sensitively detected by both CV and EIS. Notably, Cu^{2+} has been demonstrated herein for the first time as an efficient activator for $[Fe(CN)_6]^{4-}$-inactivated GO. Indeed, direct assay of $[Fe(CN)_6]^{4-}$-inhibited GO with the standard GO toolkit shows a Cu^{2+} concentration-dependent recovery of GO activity (Figure 2c, calibration curve in Figure S1). The removal of the inactivation effect of $[Fe(CN)_6]^{4-}$ by Cu^{2+} most likely results from the formation of the copper hexacyanoferrate (CuHCF) complex (*vide infra*),[31] releasing Cu at the catalytic center of GO and restoring GO back into the catalytic cycle (Figure 2d).[32]

Exploration of the Mechanism of QLA. With the QLA surface architecture created, we then proceeded to the acquisition of protein-specific glycosignature information on exosomes. Differential pulse voltammetry (DPV) is used as it provides a higher sensitivity than CV due to the enhancement of faradaic current and minimization of nonfaradaic charging current.[33] With the complete QLA surface architecture and relevant solution-phase redox probes, including H_2O_2 and hydroquinone (HQ), in place, an optimization of the buffer, pH, and Cu^{2+} concentration was performed (Figure S2a–f), with the exosome concentration fixed at 1.0×10^9 mL^{-1}. In this assay scheme, the surface-confined, localized HRP acts as the enzyme for effecting the reduction of H_2O_2, and CuHCF as well as the HQ/benzoquinone (BQ) pair acts as the mediator for shuttling electrons between HRP and the electrode (Figure 3a).[34] The number of localized HRP sites and, correspondingly, the number of remodeled MUC1-specific terminal Gal/GalNAc sites dictate the catalytically generated DPV peak current, thus allowing the achievement of QLA. The use of an acetate buffer (AB) instead of the phosphate saline buffer (PBS) is beneficial for the stabilization of Cu^{2+} and the formation of CuHCF. Indeed, an enhancement of the DPV peak current is observed in AB (Figure S2a,b). The variation of

https://dx.doi.org/10.1021/jacs.9b12182
J. Am. Chem. Soc. 2020, 142, 7404–7412

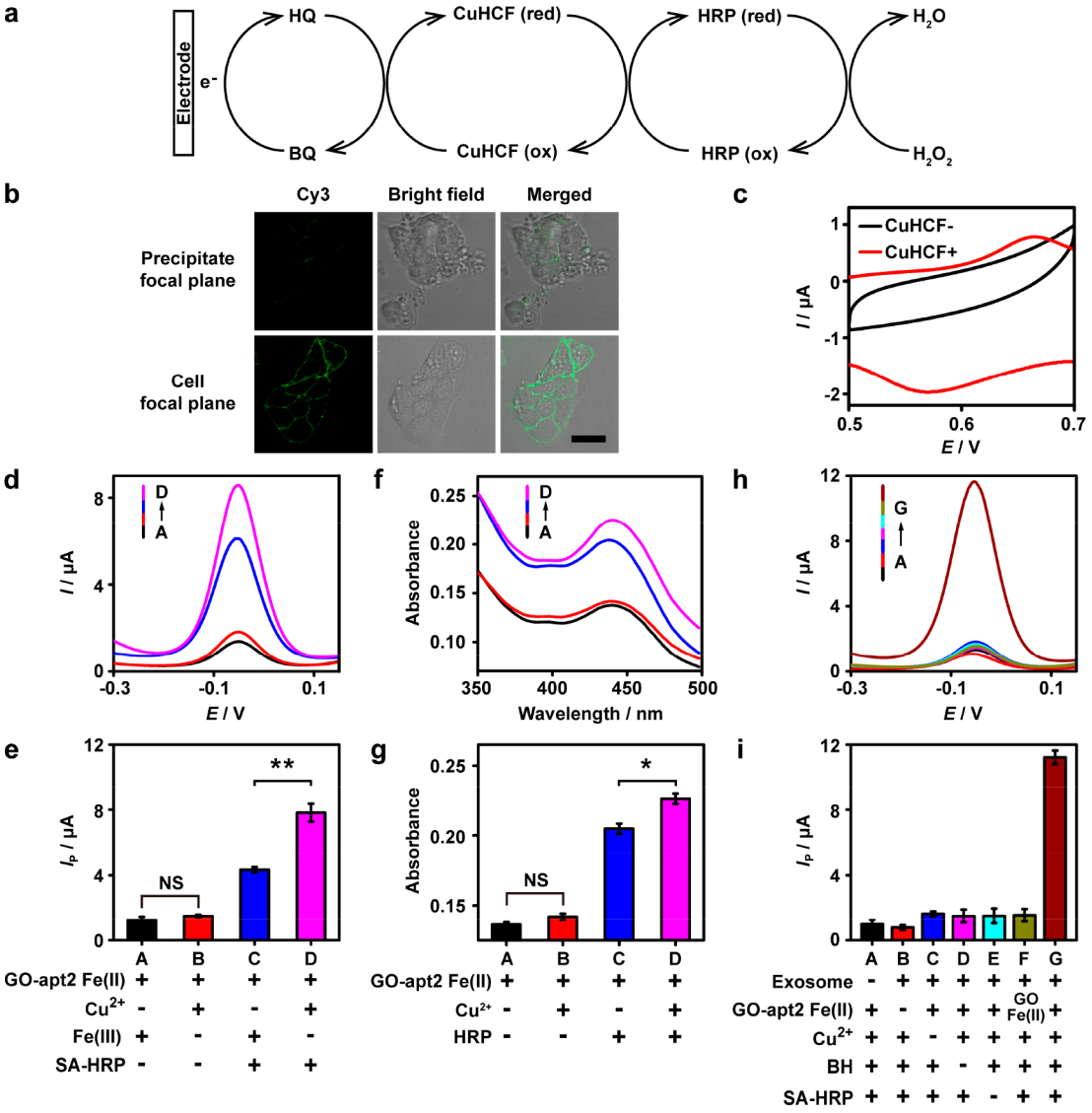

Figure 3. (a) Schematic diagram of the amplification mechanism of the QLA surface architecture. (b) Observation of the presence of CuHCF under Cu^{2+} activation. CLSM images of MCF-7 cells treated with localized chemical remodeling at a Cu^{2+} concentration of 1.0 mM from the solid precipitate focal plane and cell focal plane. Scale bar: 20 μm. (c) Electrochemical demonstration of the formation of CuHCF in QLA surface architecture. CVs of streptavidin-HRP/biotin-hydrazide/$[Fe(CN)_6]^{3-}$/GO-apt2 ($[Fe(CN)_6]^{4-}$)/BSA/exosome/MCH/5′-SH-apt1/AuE (CuHCF−) and streptavidin-HRP/biotin-hydrazide/Cu^{2+}/GO-apt2 ($[Fe(CN)_6]^{4-}$)/BSA/exosome/MCH/5′-SH-apt1/AuE (CuHCF+) in 10 mM PBS containing 0.1 M KCl. Demonstration of the electron shuttle property of CuHCF in QLA DPV: (d) DPV spectra; (e) DPV peak current values. Cu^{2+} and $[Fe(CN)_6]^{3-}$ have been optimized in concentration to maximize respective DPV signals. UV−vis absorption measurement showing the enhancement of HRP-catalyzed reaction between H_2O_2 and pyrogallol under Cu^{2+} activation: (f) UV−vis absorption spectra; (g) UV−vis peak absorption values. GO-apt2 Fe(II) here refers to the recovered product from a mixture of GO-apt2 and $[Fe(CN)_6]^{4-}$ after ultrafiltration to remove excess free $[Fe(CN)_6]^{4-}$. Demonstration of the feasibility of using DPV for the QLA evaluation of exosomal MUC1-specific terminal Gal/GalNAc: (h) DPV spectra; (i) DPV peak current values. Statistical analysis was performed with the *t* test (**$p < 0.01$; $0.01 <$ *$p < 0.05$; NS, not significant).

pH identifies an ideal value of 6.5 (Figure S2c,d). With respect to the Cu^{2+} concentration, the DPV peak current follows an initial linear increase and then plateau dependence pattern, with an inflection point at 1.0 mM (Figure S2e,f). Under these optimized conditions, a large DPV peak current can be observed. The existence of a CuHCF layer is supported by the following observations: (1) a previous study demonstrates the effectiveness of GO inhibition by $[Fe(CN)_6]^{4-}$ even after ultrafiltration removal of excess solution-phase $[Fe(CN)_6]^{4-}$, indicating the association of $[Fe(CN)_6]^{4-}$ with GO;[20] (2) localized chemical remodeling on MCF-7 cells witnesses a solid precipitate on the cell surface under bright-field microscopy when using Cu^{2+} as the activator (Figure 3b); in contrast, no precipitate is observed with the $[Fe(CN)_6]^{3-}$ activator;[20] (3) a pair of redox peaks associated with CuHCF can be observed on CV (Figure 3c).[35] The electron shuttle role of CuHCF is evident from (1) the boosted DPV peak current for HRP-catalyzed H_2O_2 reduction with the switching of activator from $[Fe(CN)_6]^{3-}$ to Cu^{2+} (Figure 3d,e) and (2) the promoted catalytic activity of HRP in a solution reaction between H_2O_2 and pyrogallol under Cu^{2+} activation (Figure 3f,g).

https://dx.doi.org/10.1021/jacs.9b12182
J. Am. Chem. Soc. 2020, 142, 7404−7412

Investigation of the Specificity of QLA. To confirm that the DPV peak is truly derived from localized chemical remodeling on exosomes, a series of control experiments were conducted (Figure 3h,i). In the absence of exosomes, GO-apt2 (along with $[Fe(CN)_6]^{4-}$), Cu^{2+}, biotin-hydrazide, or streptavidin-HRP, the DPV signal is at the background level. Also as expected, the replacement of GO-apt2 with GO generates a negligible peak DPV current. The MUC1-targeting specificity is verified by the observation of a reduced DPV peak current when the exosomal MUC1 expression level is down-regulated by transfection of the parent cells with silencing shRNA (Figure 4a–d). The terminal Gal/GalNAc remodeling specificity is corroborated by the competitive blocking of GO activity with an externally added D-Gal (abbreviated as Gal) and the corresponding diminished DPV signal (Figure 4e,f). Overall, the analytical performance of QLA is superb, showing a linear semilogarithmic dependence of DPV peak current on exosome concentration over the range of 1.0×10^6 mL^{-1} to 1.0×10^9 mL^{-1}. The limit of detection is determined to be 1.3×10^6 mL^{-1} based on the 3σ method (Figure 4g,h). As such the QLA method described herein exhibits a broader dynamic range as well as a higher sensitivity than literature-reported approaches.[36,37] The general applicability of the QLA method is demonstrated from two perspectives: (1) on two other types of exosomes, respectively from human pancreatic cancer cell line PANC-1 and lung cancer cell line A549, and (2) on *N*-glycosylated proteins, using EpCAM as the model. In the first set of experiments, the exosome- and MUC 1-dependent DPV signals are observed for both types of exosomes, which show a linear semilogarithmic relationship with exosome concentration (Figure S3a–h), while in the second set, a CD63-specific aptamer (5′-SH-apt3) is used for exosome capture, and the EpCAM-specific apt1 is used to replace apt2 for conjugating GO. The QLA displays a noticeable electrochemical signal, indicating the existence of terminal Gal/GalNAc on the *N*-glycans of MCF-7 exosome-bearing EpCAM (Figure S3i,j).

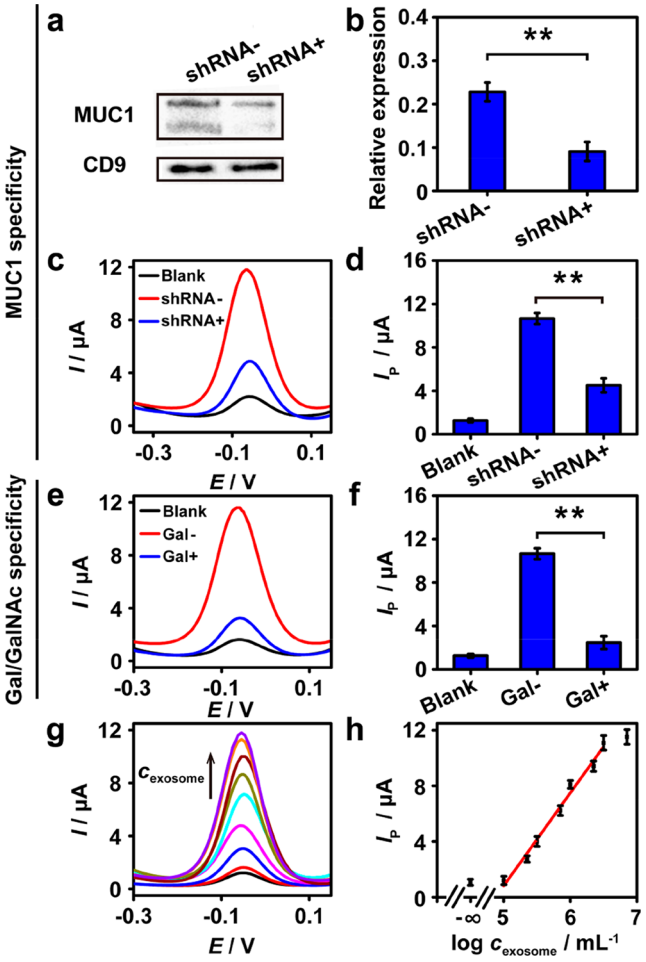

Figure 4. Assay specificity and performance of QLA. Western blot analysis of the MUC1 expression level on MCF-7 exosomes from cells after shRNA transfection: (a) Western blot diagram using CD9 as an internal reference; (b) quantification of MUC1 expression level relative to CD9 using the greyscale value from (a).[38] Demonstration of the MUC1, terminal Gal/GalNAc, and exosomal specificity by the QLA method. (c) QLA DPV signal and (d) peak current in response to the down-regulation of parent cellular MUC1 level by shRNA. (e) QLA DPV signal and (f) peak current in response to the competitive presence of Gal. (g) QLA DPV signal and (h) peak current in the presence of different concentrations of exosomes (0, 1.0×10^6, 5.0×10^6, 1.0×10^7, 5.0×10^7, 1.0×10^8, 5.0×10^8, 1.0×10^9, 5.0×10^9 mL^{-1}). Statistical analysis was performed with the *t* test (**$p < 0.01$).

Cu^{2+} Activation-Based, MUC1-Specific Gal/GalNAc Imaging on the Cell Surface. The Cu^{2+} activation format can also be applied to the localized chemical remodeling for analysis of protein-specific glycosignatures at the cellular level. For example, MUC1-specific terminal Gal/GalNAc on MCF-7 cells can be remodeled under Cu^{2+} activation, adapted with the use of streptavidin-Cy3, and subjected to fluorescence imaging with confocal laser scanning microscopy (CLSM). The optimized experimental parameters remain effective (AB, 1 mM Cu^{2+}) for maximizing the cell periphery Cy3 fluorescence signal intensity (Figure S4), with the exception of alteration of pH from 6.5 to 7.0 (Figure S5). Control experiments confirm the validity of localized chemical remodeling and therefore MUC1-specific terminal Gal/GalNAc as the source of fluorescence signal (Figure S6). Alternatively, FCM can be used as a quantitative assay method after the identical localized chemical remodeling procedure (Figure S7).

Exosomal MUC1-Specific Sialylation Capping Ratio Is Distinct from the Parent Cell Membrane. Sialylation is the covalent attachment of Sia as the terminal motif of a glycan (most frequently, capped over Gal/GalNAc via α2,3 or α2,6 linkages) and plays a critical role in cell recognition, cell signaling, and cell adhesion. Aberrant sialylation is a distinct feature defining the malignant state of the cancer.[13,39,40] With respect to our target, tumor-associated MUC1, it is highly sialylated on the cell surface, which causes premature termination of chain elongation and formation of truncated sugar branches,[28] leading to a remarkable change of the biological functions of MUC1, especially their interactions with the tumor microenvironment. Thus, we envision that assessment of the sialylation extent of MUC1 on the exosomal surface, which has a close relationship with that of cell surface MUC1, may provide a unique perspective for understanding and utilization of the glycosylation of these tumor-associated MUC1. By virtue of the unique quantitative capability of the proposed QLA, the extent of sialylation capping over MUC1-specific Gal/GalNAc (or MUC1-specific sialylation capping ratio) on exosomes can be evaluated by comparison of the QLA DPV signals before and after the cleavage of Sia with α2–3,6,8,9 neuraminidase A (sialidase) treatment[39] (Figure 5a) and calculated as $(I_2 - I_1)/(I_2 - I_0)$ (I_0: blank QLA DPV peak current with the omission of GO-apt2 ($[Fe(CN)_6]^{4-}$)/Cu^{2+} steps; I_1: QLA DPV peak current for exosomes without Sia

https://dx.doi.org/10.1021/jacs.9b12182
J. Am. Chem. Soc. 2020, 142, 7404–7412

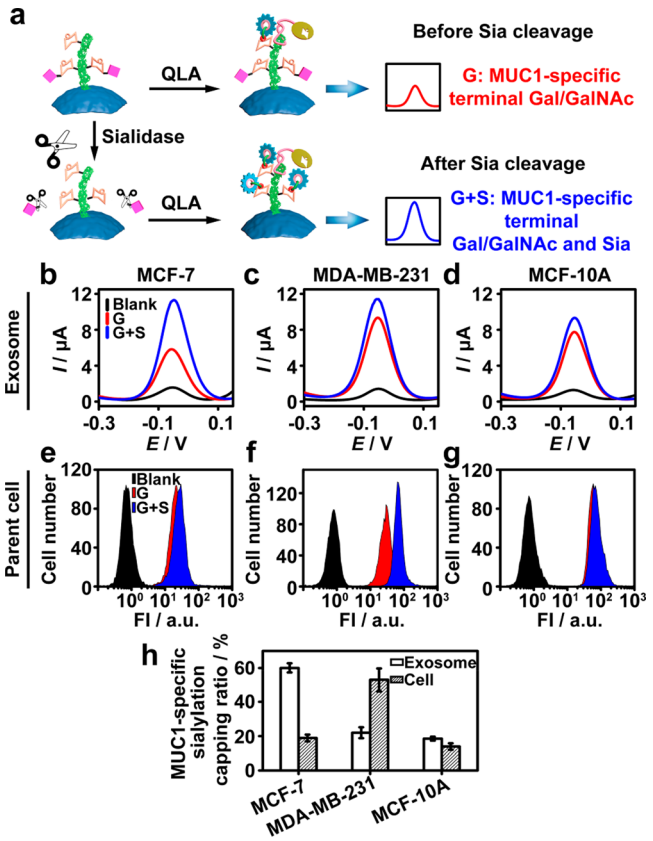

Figure 5. Analysis of exosomal and cellular MUC1-specific sialylation capping ratio. (a) Schematic illustration of the measurement principle of MUC1-specific sialylation capping ratio via QLA. QLA DPV signal for exosomal MUC1-specific terminal Gal/GalNAc before (G) and after (G+S) Sia cleavage: (b) MCF-7 exosomes, (c) MDA-MB-231 exosomes, (d) MCF-10A exosomes. FCM data for cellular MUC1-specific terminal Gal/GalNAc before (G) and after (G+S) Sia cleavage: (e) MCF-7 cells, (f) MDA-MB-231 cells, (g) MCF-10A cells. (h) Exosomal and cellular MUC1-specific sialylation capping ratio.

cleavage (G, representing MUC1-specific terminal Gal/GalNAc); I_2: QLA DPV peak current for exosomes with Sia cleavage (G+S, representing MUC1-specific terminal Gal/GalNAc and Sia)). To this end, the sialidase concentration is optimized: for MCF-7 exosomes, at a concentration of 5.0×10^7 mL^{-1}, the QLA DPV peak current reaches the plateau at a 5.0 U mL^{-1} sialidase concentration (Figure S8a). To compare the MUC1-specific sialylation capping ratio between exosomes and their parent cells, the sialidase concentration for cleaving cell surface Sia was also optimized using MDA-MB-231 cells by FCM, and a substantially higher sialidase concentration, 500 U mL^{-1}, was found to enable arrival at the plateau signal intensity (Figure S8b).

Among the three types of exosomes, the increase of the QLA DPV peak current upon Sia cleavage is most pronounced for MCF-7 exosomes (Figure 5b–d and Figure S9), while on MDA-MB-231 cells, the highest increase ratio of FCM signal is observed (Figure 5e–g and Figure S9). Consistently, MUC1-specific sialylation capping ratio analysis for MCF-7 exosomes shows a much higher value than that of MDA-MB-231 exosomes, whereas the opposite is observed for parent cells (Figure 5h). It should be noted that the calculation method of MUC1-specific sialylation capping ratio enables the comparison between exosomes of different states, between exosomes of diverse origins, and also between exosomes and cells feasible by eliminating the influence from the variation of the binding extent of apt1 or apt2. This is the first time that distinct protein-specific glycosignatures between exosomes and parent cells have been observed, which is also verified by mass spectrometry analysis (Figures S10 and S11). Considering the role of MUC1 and Sia in cell adhesion, as well as the higher metastatic capability of MDA-MB-231 cells as compared to MCF-7 cells, the MUC1-specific sialylation capping ratio is proposed to be a dictating factor modulating the metastatic potential of cancer cells and therefore a useful noninvasive indicator for subtyping cancer cells. This proposal is further supported by the low MUC1-specific sialylation capping ratios for both MCF-10A cells and MCF-10A exosomes. The above results also suggest that part of the function of exosome secretion is likely to preserve the cellular compositional and functional integrity. The high metastatic activity of MDA-MB-231 cells is achieved through the disposal of lowly sialylated MUC1 on released exosomes and therefore maintenance of a high MUC1-specific sialylation level. The opposite is true for the lowly metastatic MCF-7 cells.

Investigation of the Biogenesis Pathway of Exosomes. To date, the most intensive study of the exosome formation has revealed their intracellular endocytic trafficking pathway (Figure 6a). In addition to this "classical pathway" of exosome formation, there is also a direct exosome formation pathway (Figure 6a).[41] For example, T cells and erythroleukemia cell lines release exosomes directly from the plasma membrane.[41,42] The mechanism behind the selection principle for cells to release exosomes is largely unknown, and thus development of a facile method that facilitates the distinction of the two pathways is beneficial. To this end, we use sialidase to cleave the Sia on parent cells (which is referred to as PC–Sia cleavage to differentiate this step from the one involved in obtaining MUC1-specific sialylation capping ratio) and compare the MUC1-specific sialylation capping ratio before and after manipulation on both cells and exosomes (Figure 6). We hypothesize that if the exosomes are released by the direct pathway, the variation trends for cells and exosomes would be parallel; otherwise, different trends would be observed. As expected, the PC–Sia cleavage causes almost complete depletion of Sia on the cell surface (Figure 6c,h,l). Only a slight increase of the MUC1-specific sialylation capping ratio is observed on the cell surface after an 8 h recovery period (Figure 6d,i,l), which rises to the level of just 34.7% (MCF-7) and 28.9% (MDA-MB-231) of those for cells collected 8 h before PC–Sia cleavage (Figure 6b,g,l). In contrast, the MUC1-specific sialylation capping ratio of exosomes collected 8 h after PC–Sia cleavage remains at 89.9% (MCF-7) and 74.5% (MDA-MB-231) of those observed on exosomes collected before manipulation (Figure 6e,f,j,k,m). Therefore, we can infer to some extent that the exosomes of MCF-7 and MDA-MB-231 are not directly derived from the plasma membrane, but are secreted by the "classical pathway". This inference is further supported by the obviously different protein profiles of exosomes compared with those of the corresponding parent cells (Figure S12). Overall, by comparing the MUC1-specific sialylation capping ratio change trends between parent cells and exosomes, we provide a facile method to discriminate exosome biogenesis pathways.

https://dx.doi.org/10.1021/jacs.9b12182
J. Am. Chem. Soc. 2020, 142, 7404–7412

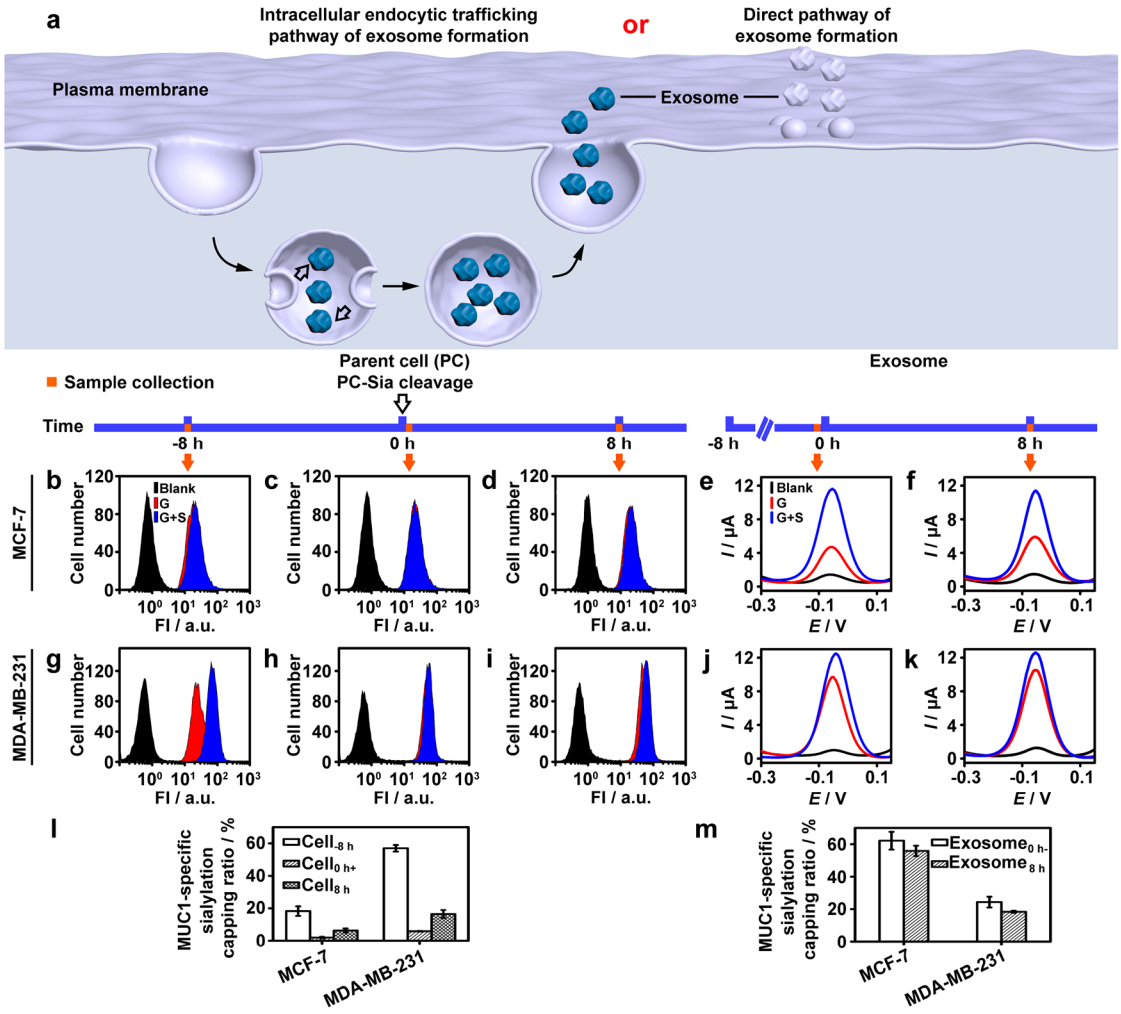

Figure 6. Revelation of exosome biogenesis pathway. (a) Exosome biogenesis pathways: classic intracellular endocytic trafficking pathway and direct pathway. FCM data for cellular MUC1-specific terminal Gal/GalNAc before (G) and after (G+S) Sia cleavage: (b–d) MCF-7 cells and (g–i) MDA-MB-231 cells collected (b, g) 8 h before, (c, h) 0 h after, and (d, i) 8 h after PC-Sia cleavage. QLA DPV signal for exosomal MUC1-specific terminal Gal/GalNAc before (G) and after (G+S) Sia cleavage: (e, f) MCF-7 exosomes and (j, k) MDA-MB-231 exosomes collected (e, j) before and (f, k) 8 h after PC-Sia cleavage. Tracking changes of (l) cellular and (m) exosomal MUC1-specific sialylation capping ratio.

CONCLUSION

In summary, a QLA method has been developed for the assay of protein-specific glycosignatures on exosomes, which is customized to meet the assay challenges for the small-sized and free-floating exosomes by integrating localized chemical remodeling with quantitative electrochemistry. The proposed method allows the first-time revelation of distinct MUC1-specific sialylation capping ratios on extracellular vesicles as compared to parent cells. Considering that the content on the exosomal surface is determined by the sorting mechanisms involved in exosomal biogenesis, the observed enrichment of a certain protein subtype with destined sialylation capping ratio indicates that glycosylation, at least in part, participates in the biogenesis of exosomes, which is beyond the well-characterized machinery based on the endosomal sorting complex required for transport (ESCRT). It is well recognized that glycosylation plays an important role in protein trafficking to specific membrane domains,[43] such as the classical apical to basolateral protein-trafficking protein-sorting pathway, where multiple glycosylation and other sorting signals are in effect and are protein-specific.[44,45] However, the glycan-based exosomal recruitment and sorting mechanisms are not well understood,[15,46] which might involve some intracellular glycan-recognizing proteins such as galectins.[47,48] Our results suggest that protein-specific glycosignatures may serve as sorting motifs for exosomes and that we cannot simply extend cellular glycosignatures to exosomes, but protein-specific scrutinization is required. The modular adaptability of a localized chemical remodeling scheme and the miniaturization compatibility of the electrochemical system should enable the comprehensive QLA profiling of glycoproteins of different types and different exosomal origins, which will contribute to the understanding of glycosignature-regulated mechanisms involved in exosomal biogenesis, release, and interactions with cells.

ASSOCIATED CONTENT

Supporting Information

The Supporting Information is available free of charge at https://pubs.acs.org/doi/10.1021/jacs.9b12182.

Experimental procedures and supplementary figures (PDF)

https://dx.doi.org/10.1021/jacs.9b12182
J. Am. Chem. Soc. 2020, 142, 7404–7412

AUTHOR INFORMATION

Corresponding Author

Lin Ding − *State Key Laboratory of Analytical Chemistry for Life Science, School of Chemistry and Chemical Engineering and Chemistry and Biomedicine Innovation Center (ChemBIC), Nanjing University, Nanjing 210023, China;* orcid.org/0000-0001-5381-3484; Email: dinglin@nju.edu.cn

Authors

Yuna Guo − *State Key Laboratory of Analytical Chemistry for Life Science, School of Chemistry and Chemical Engineering, Nanjing University, Nanjing 210023, China*

Jing Tao − *State Key Laboratory of Analytical Chemistry for Life Science, School of Chemistry and Chemical Engineering, Nanjing University, Nanjing 210023, China*

Yiran Li − *State Key Laboratory of Analytical Chemistry for Life Science, School of Chemistry and Chemical Engineering, Nanjing University, Nanjing 210023, China*

Yimei Feng − *State Key Laboratory of Analytical Chemistry for Life Science, School of Chemistry and Chemical Engineering, Nanjing University, Nanjing 210023, China*

Huangxian Ju − *State Key Laboratory of Analytical Chemistry for Life Science, School of Chemistry and Chemical Engineering, Nanjing University, Nanjing 210023, China;* orcid.org/0000-0002-6741-5302

Zhongfu Wang − *Key Laboratory of Resource Biology and Biotechnology in Western China, Ministry of Education and Provincial Key Laboratory of Biotechnology, College of Life Sciences, Northwest University, Xi'an 710069, China;* orcid.org/0000-0003-1616-5056

Complete contact information is available at: https://pubs.acs.org/10.1021/jacs.9b12182

Notes

The authors declare no competing financial interest.

ACKNOWLEDGMENTS

We would like to thank Prof. Jianping Lei (Nanjing University) for helpful discussions and Prof. Yang Mao (Sun Yat-sen University) for advice and expertise. We also gratefully acknowledge support from the National Natural Science Foundation of China (21974067, 21675082), the National Key Research and Development Program of China (2018YFC1004704), Fundamental Research Funds for the Central Universities (020514380184), and State Key Laboratory of Analytical Chemistry for Life Science (5431ZZXM1903).

REFERENCES

(1) Pluchino, S.; Smith, J. A. Explicating exosomes: reclassifying the rising stars of intercellular communication. *Cell* **2019**, *177*, 225−227.

(2) Mathieu, M.; Martin-Jaular, L.; Lavieu, G.; Théry, C. Specificities of secretion and uptake of exosomes and other extracellular vesicles for cell-to-cell communication. *Nat. Cell Biol.* **2019**, *21*, 9−17.

(3) Takahashi, A.; Okada, R.; Nagao, K.; Kawamata, Y.; Hanyu, A.; Yoshimoto, S.; Takasugi, M.; Watanabe, S.; Kanemaki, M. T.; Obuse, C.; Hara, E. Exosomes maintain cellular homeostasis by excreting harmful DNA from cells. *Nat. Commun.* **2017**, *8*, 15287.

(4) Wolfers, J.; Lozier, A.; Raposo, G.; Regnault, A.; Théry, C.; Masurier, C.; Flament, C.; Pouzieux, S.; Faure, F.; Tursz, T.; Angevin, E.; Amigorena, S.; Zitvogel, L. Tumor-derived exosomes are a source of shared tumor rejection antigens for CTL cross-priming. *Nat. Med.* **2001**, *7*, 297−303.

(5) Sharma, P.; Mesci, P.; Carromeu, C.; McClatchy, D. R.; Schiapparelli, L.; Yates, J. R., III; Muotri, A. R.; Cline, H. T. Exosomes regulate neurogenesis and circuit assembly. *Proc. Natl. Acad. Sci. U. S. A.* **2019**, *116*, 16086−16094.

(6) Zhao, L.; Liu, W. T.; Xiao, J.; Cao, B. W. The role of exosomes and "exosomal shuttle microRNA" in tumorigenesis and drug resistance. *Cancer Lett.* **2015**, *356*, 339−346.

(7) Liu, C.; Zhao, J. X.; Tian, F.; Cai, L. L.; Zhang, W.; Feng, Q.; Chang, J. Q.; Wan, F. N.; Yang, Y. J.; Dai, B.; Cong, Y. L.; Ding, B. Q.; Sun, J. S.; Tan, W. H. Low-cost thermophoretic profiling of extracellular-vesicle surface proteins for the early detection and classification of cancers. *Nat. Biomed Eng.* **2019**, *3*, 183−193.

(8) Kamerkar, S.; LeBleu, V. S.; Sugimoto, H.; Yang, S.; Ruivo, C. F.; Melo, S. A.; Lee, J. J.; Kalluri, R. Exosomes facilitate therapeutic targeting of oncogenic KRAS in pancreatic cancer. *Nature* **2017**, *546*, 498−503.

(9) Skotland, T.; Sandvig, K. The role of PS 18:0/18:1 in membrane function. *Nat. Commun.* **2019**, *10*, 2752.

(10) Alexander, M.; Hu, R.; Runtsch, M. C.; Kagele, D. A.; Mosbruger, T. L.; Tolmachova, T.; Seabra, M. C.; Round, J. L.; Ward, D. M.; O'Connell, R. M. Exosome-delivered microRNAs modulate the inflammatory response to endotoxin. *Nat. Commun.* **2015**, *6*, 7321.

(11) Taylor, D. D.; Gercel-Taylor, C. Exosomes/microvesicles: mediators of cancer-associated immunosuppressive microenvironments. *Semin. Immunopathol.* **2011**, *33*, 441−454.

(12) Théry, C.; Zitvogel, L.; Amigorena, S. Exosomes: composition, biogenesis and function. *Nat. Rev. Immunol.* **2002**, *2*, 569−579.

(13) Stowell, S. R.; Ju, T. Z.; Cummings, R. D. Protein glycosylation in cancer. *Annu. Rev. Pathol.: Mech. Dis.* **2015**, *10*, 473−510.

(14) Costa, J. Glycoconjugates from extracellular vesicles: Structures, functions and emerging potential as cancer biomarkers. *Biochim. Biophys. Acta, Rev. Cancer* **2017**, *1868*, 157−166.

(15) Batista, B. S.; Eng, W. S.; Pilobello, K. T.; Hendricks-Muñoz, K. D.; Mahal, L. K. Identification of a conserved glycan signature for microvesicles. *J. Proteome Res.* **2011**, *10*, 4624−4633.

(16) Melo, S. A.; Luecke, L. B.; Kahlert, C.; Fernandez, A. F.; Gammon, S. T.; Kaye, J. V.; LeBleu, S. E.; Mittendorf, A.; Weitz, J.; Rahbari, N.; Reissfelder, C.; Pilarsky, C.; Fraga, M. F.; Piwnica-Worms, D.; Kalluri, R. Glypican-1 identifies cancer exosomes and detects early pancreatic cancer. *Nature* **2015**, *523*, 177−182.

(17) Krishnamoorthy, L.; Bess, J. W., Jr; Preston, A. B.; Nagashima, K.; Mahal, L. K. HIV-1 and microvesicles from T cells share a common glycome, arguing for a common origin. *Nat. Chem. Biol.* **2009**, *5*, 244−250.

(18) Feng, Y. M.; Guo, Y. N.; Li, Y. R.; Tao, J.; Ding, L.; Wu, J.; Ju, H. X. Lectin-mediated in situ rolling circle amplification on exosomes for probing cancer-related glycan pattern. *Anal. Chim. Acta* **2018**, *1039*, 108−115.

(19) Bertozzi, C. R.; Kiessling, L. L. Chemical glycobiology. *Science* **2001**, *291*, 2357−2364.

(20) Hui, J. J.; Bao, L.; Li, S. Q.; Zhang, Y.; Feng, Y. M.; Ding, L.; Ju, H. X. Localized chemical remodeling for live cell imaging of protein-specific glycoform. *Angew. Chem., Int. Ed.* **2017**, *56*, 8139−8143.

(21) Haga, Y.; Ishii, K.; Hibino, K.; Sako, Y.; Ito, Y.; Taniguchi, N.; Suzuki, T. Visualizing specific protein glycoforms by transmembrane fluorescence resonance energy transfer. *Nat. Commun.* **2012**, *3*, 907.

(22) Lin, W.; Du, Y. F.; Zhu, Y. T.; Chen, X. A cis-membrane FRET-based method for protein-specific imaging of cell-surface glycans. *J. Am. Chem. Soc.* **2014**, *136*, 679−687.

(23) Yang, Y. T.; Shen, G. X.; Wang, H.; Li, H. X.; Zhang, T.; Tao, N. J.; Ding, X. T.; Yu, H. Interferometric plasmonic imaging and detection of single exosomes. *Proc. Natl. Acad. Sci. U. S. A.* **2018**, *115*, 10275−10280.

(24) Liu, Y.; Tseng, Y.-c.; Huang, L. Biodistribution studies of nanoparticles using fluorescence imaging: a qualitative or quantitative method? *Pharm. Res.* **2012**, *29*, 3273−3277.

(25) Dong, H. L.; Chen, H. F.; Jiang, J. Q.; Zhang, H.; Cai, C. X.; Shen, Q. M. Highly sensitive electrochemical detection of tumor

exosomes based on aptamer recognition-induced multi-DNA release and cyclic enzymatic amplification. *Anal. Chem.* **2018**, *90*, 4507−4513.
(26) Melo, S. A.; Sugimoto, H.; O'Connell, J. T.; Kato, N.; Villanueva, A.; Vidal, A.; Qiu, L.; Vitkin, E.; Perelman, L. T.; Melo, C. A.; Lucci, A.; Ivan, C.; Calin, G. A.; Kalluri, R. Cancer exosomes perform cell-independent microRNA biogenesis and promote tumorigenesis. *Cancer Cell* **2014**, *26*, 707−721.
(27) Shao, H. L.; Im, H.; Castro, C. M.; Breakefield, X.; Weissleder, R.; Lee, H. New technologies for analysis of extracellular vesicles. *Chem. Rev.* **2018**, *118*, 1917−1950.
(28) Nath, S.; Mukherjee, P. MUC1: a multifaceted oncoprotein with a key role in cancer progression. *Trends Mol. Med.* **2014**, *20*, 332−342.
(29) Wang, S.; Zhang, L. Q.; Wan, S.; Cansiz, S.; Cui, C.; Liu, Y.; Cai, R.; Hong, C. Y.; Teng, I.-T.; Shi, M. L.; Wu, Y.; Dong, Y. Y.; Tan, W. H. Aptasensor with expanded nucleotide using DNA nanotetrahedra for electrochemical detection of cancerous exosomes. *ACS Nano* **2017**, *11*, 3943−3949.
(30) Ferreira, C. S. M.; Matthews, C. S.; Missailidis, S. DNA aptamers that bind to MUC1 tumour marker: design and characterization of MUC1-binding single-stranded DNA aptamers. *Tumor Biol.* **2006**, *27*, 289−301.
(31) Kitis, M.; Akcil, A.; Karakaya, E.; Yigit, N. O. Destruction of cyanide by hydrogen peroxide in tailings slurries from low bearing sulphidic gold ores. *Miner. Eng.* **2005**, *18*, 353−362.
(32) Hamilton, G. A.; Adolf, P. K.; de Jersey, J.; DuBois, G. C.; Dyrkacz, G. R.; Libby, R. D. Trivalent copper, superoxide, and galactose oxidase. *J. Am. Chem. Soc.* **1978**, *100*, 1899−1912.
(33) Skoog, D. A.; Holler, F. J.; Crouch, S. R. *Principles of Instrumental Analysis*, 6th ed.; Thomson Brooks/Cole: Belmont, CA, 2007; p 743.
(34) Zhang, T. J.; Wang, W.; Zhang, D. Y.; Zhang, X. X.; Ma, Y. R.; Zhou, Y. L.; Qi, L. M. Biotemplated synthesis of gold nanoparticle−bacteria cellulose nanofiber nanocomposites and their application in biosensing. *Adv. Funct. Mater.* **2010**, *20*, 1152−1160.
(35) Pauliukaite, R.; Brett, C. M. A. Characterization of novel glucose oxysilane sol-gel electrochemical biosensors with copper hexacyanoferrate mediator. *Electrochim. Acta* **2005**, *50*, 4973−4980.
(36) Wang, Y.-M.; Liu, J.-W.; Adkins, G. B.; Shen, W.; Trinh, M. P.; Duan, L.-Y.; Jiang, J.-H.; Zhong, W. W. Enhancement of the intrinsic peroxidase-like activity of graphitic carbon nitride nanosheets by ssDNAs and its application for detection of exosomes. *Anal. Chem.* **2017**, *89*, 12327−12333.
(37) Park, J.; Hwang, M.; Choi, B.; Jeong, H.; Jung, J. H.; Kim, H. K.; Hong, S.; Park, J. H.; Choi, Y. Exosome classification by pattern analysis of surface-enhanced raman spectroscopy data for lung cancer diagnosis. *Anal. Chem.* **2017**, *89*, 6695−6701.
(38) Li, S. Q.; Liu, Y. R.; Liu, L.; Feng, Y. M.; Ding, L.; Ju, H. X. A hierarchical coding strategy for live cell imaging of protein-specific glycoform. *Angew. Chem., Int. Ed.* **2018**, *57*, 12007−12011.
(39) Pearce, O. M. T.; Läubli, H. Sialic acids in cancer biology and immunity. *Glycobiology* **2016**, *26*, 111−128.
(40) Wang, L. B.; Liu, Y.; Wu, L. J.; Sun, X.-L. Sialyltransferase inhibition and recent advances. *Biochim. Biophys. Acta, Proteins Proteomics* **2016**, *1864*, 143−153.
(41) van der Pol, E.; Böing, A. N.; Harrison, P.; Sturk, A.; Nieuwland, R. Classification, functions, and clinical relevance of extracellular vesicles. *Pharmacol. Rev.* **2012**, *64*, 676−705.
(42) Booth, A. M.; Fang, Y.; Fallon, J. K.; Yang, J.-M.; Hildreth, J. E.K.; Gould, S. J. Exosomes and HIV Gag bud from endosome-like domains of the T cell plasma membrane. *J. Cell Biol.* **2006**, *172*, 923−935.
(43) Liang, Y.; Eng, W. S.; Colquhoun, D. R.; Dinglasan, R. R.; Graham, D. R.; Maha, L. K. Complex *N*-linked glycans serve as a determinant for exosome/microvesicle cargo recruitment. *J. Biol. Chem.* **2014**, *289*, 32526−32537.
(44) Delacour, D.; Cramm-Behrens, C. I.; Drobecq, H.; Le Bivic, A.; Naim, H. Y.; Jacob, R. Requirement for galectin-3 in apical protein sorting. *Curr. Biol.* **2006**, *16*, 408−414.
(45) Mattila, P. E.; Youker, R. T.; Mo, D.; Bruns, J. R.; Cresawn, K. O.; Hughey, R. P.; Ihrke, G.; Weisz, O. A. Multiple biosynthetic trafficking routes for apically secreted proteins in MDCK cells. *Traffic* **2012**, *13*, 433−442.
(46) Gerlach, J. Q.; Griffin, M. D. Getting to know the extracellular vesicle glycome. *Mol. BioSyst.* **2016**, *12*, 1071−1081.
(47) Barres, C.; Blanc, L.; Bette-Bobillo, P.; Andre, S.; Mamoun, R.; Gabius, H. J.; Vidal, M. Galectin-5 is bound onto the surface of rat reticulocyte exosomes and modulates vesicle uptake by macrophages. *Blood* **2010**, *115*, 696−705.
(48) Moreno-Gonzalo, O.; Villarroya-Beltri, C.; Sanchez-Madrid, F. Post-translational modifications of exosomal proteins. *Front. Immunol.* **2014**, *5*, 383.

https://dx.doi.org/10.1021/jacs.9b12182
J. Am. Chem. Soc. 2020, 142, 7404−7412